

A record-high ocean bottom pressure in the South Pacific observed by GRACE

Carmen Boening,¹ Tong Lcc,¹ and Victor Zlotnicki¹

Received 29 October 2010; revised 24 November 2010; accepted 22 December 2010; published 17 February 2011.

[1] In late 2009 to early 2010, the Gravity Recovery and Climate Experiment (GRACE) satellite pair observed a record increase in ocean bottom pressure (OBP) over a large mid-latitude region of the South East Pacific. Its magnitude is substantially larger than other oceanic events in the Southern Hemisphere found in the entire GRACE data records (2003–2010) on multi-month time scales. The OBP data help to understand the nature of a similar signal in sea surface height (SSH) anomaly observed by altimetry: the SSH increase is mainly due to mass convergence. Analysis of the barotropic vorticity equation using scatterometer data, atmospheric reanalysis product, and GRACE and altimeter an atmospheric reanalysis product observations suggests that the observed OBP/SSH signal was primarily caused by wind stress curl associated with a strong and persistent anticyclone in late 2009 in combination with effects of planetary vorticity gradient, bottom topography, and friction. **Citation:** Boening, C., T. Lee, and V. Zlotnicki (2011), A record-high ocean bottom pressure in the South Pacific observed by GRACE, *Geophys. Res. Lett.*, 38, L04602, doi:10.1029/2010GL046013.

1. Introduction

[2] The Gravity Recovery and Climate Experiment (GRACE) provides estimates of the time-varying gravity field since late 2002. Many science applications addressing changes in the Earth's mass redistribution have benefited from this unprecedented data set. GRACE data have been used to study mass loss from ice sheets [Velicogna, 2009], groundwater storage and change [e.g., Syed *et al.*, 2008], and global scale sea level change [Willis *et al.*, 2008]. Gravity field anomalies predominantly reflect water mass redistribution on the Earth's surface. Over the ocean, gravity field anomalies not caused by the solid earth are associated with changes in ocean bottom pressure (OBP), i.e. the pressure exerted on the ocean floor by the water column and the overlying atmosphere. Anomalies in OBP can be induced by local mass re-distribution as a result of changes in wind-forced ocean circulation. Seasonal fluctuations in the global hydrological cycle [e.g., Chambers *et al.*, 2004] and atmospheric pressure over the ocean [Ponte, 1999] also contribute to OBP variability.

[3] The detection of local fluctuations in OBP from GRACE gravity field solutions is subject to two major difficulties. First, gravity signals associated with water mass distribution within the ocean are much smaller than land

signals. The hydrologic cycle over the Amazon Basin for example has an annual amplitude of about 24 cm [Syed *et al.*, 2008], whereas typical changes in OBP on a monthly scale are only up to 5 cm [Macrander *et al.*, 2010]. The small amplitude of oceanic signals decreases the signal-to-noise ratio in the data sets and renders the detection of local oceanic variability difficult. Another difficulty arises near the coasts because of the large amplitude difference between land and ocean signals. The larger land signals “leak” into the ocean signals due to the relatively coarse spatial resolution (a few hundred kilometers), complicating the analysis of coastal oceanic signals.

[4] Despite these difficulties, there have been a number of oceanographic applications of GRACE data. For example, GRACE data have been used along with other observations to investigate global sea level change [Willis *et al.*, 2008], volume transport variations of the Antarctic Circumpolar Current [e.g., Zlotnicki *et al.*, 2007; Ponte and Quinn, 2009], and variability in the North Pacific [Chambers and Willis, 2008].

[5] In this study, we report a record-high OBP signal in the South East Pacific (SEP) using GRACE data, and examine the forcing mechanisms using GRACE in conjunction with measurements from a satellite scatterometer and altimeters as well as from an atmospheric reanalysis product. Our study, being an additional demonstration of the application of GRACE data to study oceanic signals, is one of the few efforts that characterize sub-basin scale oceanic features [Zlotnicki *et al.*, 2007; Ponte and Quinn, 2009; Chambers and Willis, 2008]. In addition to describing the record high OBP signal, we provide a dynamical explanation of the forcing mechanism based on multi-sensor satellite observations.

2. Data

2.1. GRACE Data

[6] We used gridded ocean bottom pressure fields derived from monthly GRACE CSR RL04 solutions available from <http://grace.jpl.nasa.gov/data/mass/>, which are post-processed based on Chambers [2006]. The data are available for the time period from 2003–2010. The post-processing includes a correction for geocenter motion, replacement of the spherical harmonic coefficient C(2,0) with one derived from laser tracking, destriping and Gaussian filters, an iterative process to remove land leakage, and post glacial rebound.

2.2. Altimeter Data

[7] We also analyzed measurements of sea surface height (SSH) anomaly derived from the TOPEX/POSEIDON (October 1992 to October 2005) and JASON-1 (January 2001 to present) and JASON-2 (June 2008 to present) altimeter missions. For the overlapping period between any two

¹Jet Propulsion Laboratory, California Institute of Technology, Pasadena, California, USA.

missions, data from the newer mission are used. A bias correction was applied to the JASON-1 and 2 data to produce a continuous and consistent time series of SSH anomaly from the satellite missions. These data were processed in-house at JPL. High-frequency variability in SSH at high-latitude oceans is often barotropic (thus reflecting OBP changes). Therefore, the comparison between the GRACE and altimeter data not only serves as a consistency check, but also helps to understand the nature of the SSH signal.

2.3. Scatterometer Data

[8] Ocean surface vector wind data from the Advanced Scatterometer (ASCAT) instrument aboard the MetOp-A platform (February 2007 to present) were used to investigate the forcing of the OBP and SSH. The ASCAT swath data [Verspeek *et al.*, 2010] were processed by the Ocean and Sea Ice Satellite Application Facility (OSI SAF) and distributed by the Royal Netherlands Meteorological Institute (KNMI) and NASA's Physical Oceanography Distributed Active Archived Center (PO.DAAC, <http://podaac.jpl.nasa.gov>). The ASCAT swath product (wind speed, direction) was converted to daily averages of wind stress on a $0.5^\circ \times 0.5^\circ$ grid. Following Risien and Chelton [2006], daily wind vectors are computed by vector averaging $\mathbf{u} = (u, v)$ over the previous three days, then computing daily stresses according to

$$\tau_x = \rho_a c_d |\mathbf{u}| u; \tau_y = \rho_a c_d |\mathbf{u}| v, \quad (1)$$

where ρ_a is the air density. The drag coefficients c_d were determined as a function of wind speed using the relation described by Smith [1988]. Monthly means of wind stress τ_x , τ_y are calculated from the daily wind stress.

2.4. Atmospheric Reanalysis

[9] We also analyzed the National Center for Environmental Prediction (NCEP) and Department of Energy (DOE) reanalysis II product from 1979–2009 (hereafter NCEP) [Kanamitsu *et al.*, 2002]. The NCEP wind vectors are similarly converted to wind stress using the same drag-coefficient formula from Smith [1988]. The longer record of the NCEP product allows us to examine how anomalous the wind forcing in late 2009 was compared to those in the past three decades.

2.5. Bathymetric Data

[10] The bathymetry was derived from the ETOPO5 global elevation database [National Oceanic and Atmospheric Administration, 1988], which is available on a $1/12^\circ \times 1/12^\circ$ grid. The data were smoothed and re-gridded on a $1^\circ \times 1^\circ$ grid.

3. Results

[11] Maps of OBP anomaly (referenced to 2003–2008 monthly seasonal climatology) derived from GRACE show a record increase in the SEP during late 2009/early 2010 (color shading in Figures 1a–1d). At its peak, the anomaly covers the region between 90° – 140° W, 35° – 55° S with a center around 120° W. The maximum amplitude (6–8 cm in Nov. 09) exceeds the standard deviation of the monthly time series by a factor of four, and is the largest multi-month southern-hemisphere oceanic signal found in the entire

GRACE data record from 2003 to 2010. The ocean model (OMCT) that was used to de-alias GRACE is found to be inadequate in representing the amplitude and phase of the record anomaly (Figure S1 of the auxiliary material).¹

[12] Variations of altimeter-derived SSH anomalies in this region are also examined. Changes in SSH are either related to steric changes (i.e., changes in water column density caused by temperature or salinity fluctuations) or to changes in mass, i.e. OBP. Analyzing SSH changes in relation to OBP changes thus provides information about the relative contributions of mass and steric changes to the SSH signal. Maps of SSH anomalies (also referenced to the 2003–2008 monthly seasonal climatology) show an increase in the SEP (black contours in Figures 1a–1d) that is nearly coincident with the OBP signal. Moreover, the spatial extent and amplitude agree well with the OBP observations.

[13] To further quantify the extent of agreement between OBP and SSH, we examined the temporal evolution of OBP and SSH changes. The time series of OBP anomalies averaged over the SEP box (defined as 90° – 140° W, 35° – 55° S) is very similar to the counterpart for the SSH anomaly (Figure 1e). The correlation between SSH and OBP 2003–2010 time series is 0.79 (significant at a 99% confidence level). The OBP signal explains about 58% of the SSH variance indicating that a significant part of sea level anomalies in this region are due to mass changes. In 2009–2010 the correlation of SSH and OBP reaches 0.97, with 94% of the variance in the SSH signal being explained by OBP. This indicates that the large SSH increase in late 2009 is related to mass convergence (as opposed to density changes). Examination of the entire altimeter data record suggests that this increase is also a record high for the SEP region since 1992 (not shown).

[14] To examine the potential forcing mechanisms for the OBP and SSH signals, we analyzed wind stress and wind stress curl derived from the ASCAT data. Maps of monthly mean wind stress anomalies (referenced to a monthly “seasonal climatology” for the period of April 2007 to April 2010, the period over which ASCAT data are available) show enhanced amplitudes in the South East to South Central Pacific (vectors in Figures 2a–2d). The corresponding anomalously high (positive) wind stress curl near the SEP (color shading in Figures 2a–2d) could be a potential forcing of the record-high SSH (OBP). The NCEP product shows that wind stress curl averaged over the SEP region reached a three-decade high in late 2009, reflecting the extremely strong and persistent anticyclone (Figure S2) that corresponds to the record high OBP.

[15] To quantify the dominant atmospheric forcing mechanism and the oceanic response process, we analyze the barotropic vorticity balance [see Fu and Davidson, 1995; Vivier *et al.*, 2005] as described by the following equation:

$$\begin{aligned} \frac{\partial}{\partial t} \nabla^2 \eta - \frac{f^2}{gH} \frac{\partial \eta}{\partial t} + \beta \frac{\partial \eta}{\partial x} - \frac{f}{H} \left(\frac{\partial \eta}{\partial x} \frac{\partial H}{\partial y} - \frac{\partial \eta}{\partial y} \frac{\partial H}{\partial x} \right) + \nabla \cdot \left(\frac{r}{H} \nabla \eta \right) \\ = \frac{f}{\rho g} \nabla \times \frac{\tau}{H} - \frac{f^2}{g^2 H \rho} \frac{\partial P_a}{\partial t} \end{aligned} \quad (2)$$

¹Auxiliary materials are available in the HTML. doi:10.1029/2010GL046013.

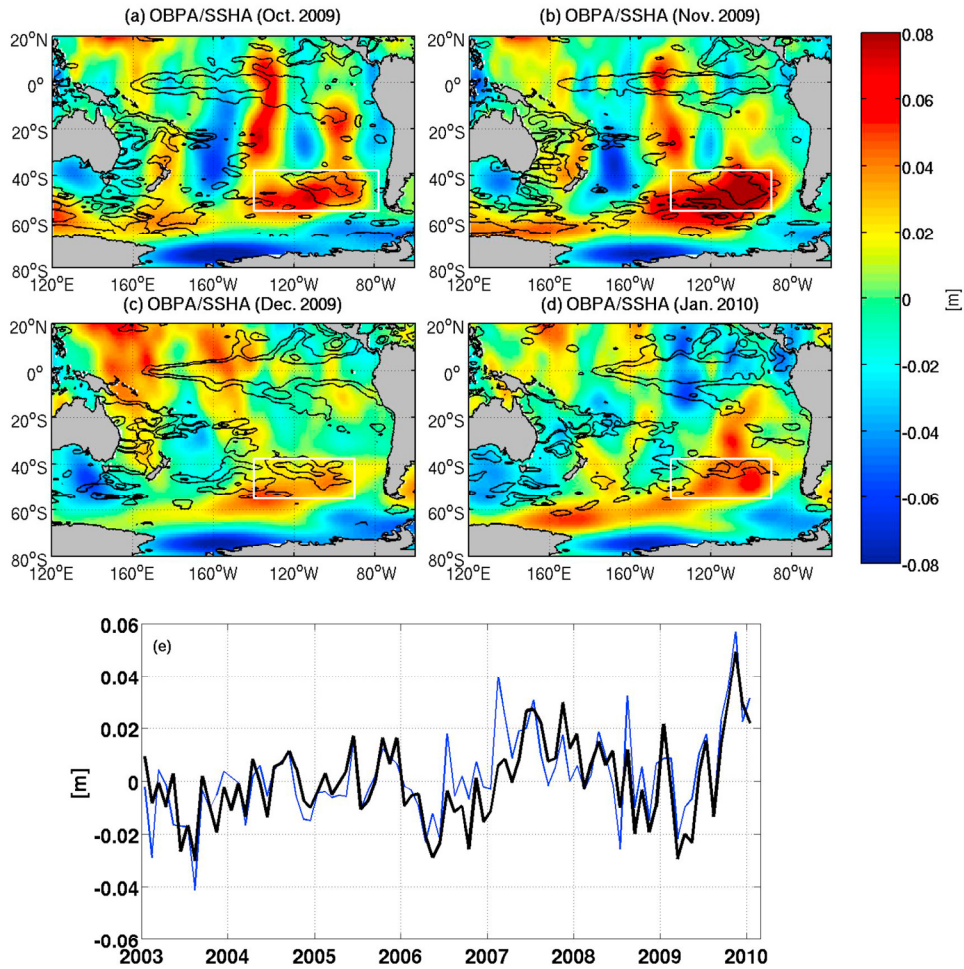


Figure 1. (a–d) Maps of monthly means of OBP anomalies derived from GRACE (2003–2008 climatology removed). Overlying contours indicate SSH anomalies at 4 cm and 8 cm from TOPEX/Poseidon, Jason I altimetry during the respective months. (e) Time series of OBP (blue) and SSH (black) anomalies averaged over 90°–140°W, 35°–55°S.

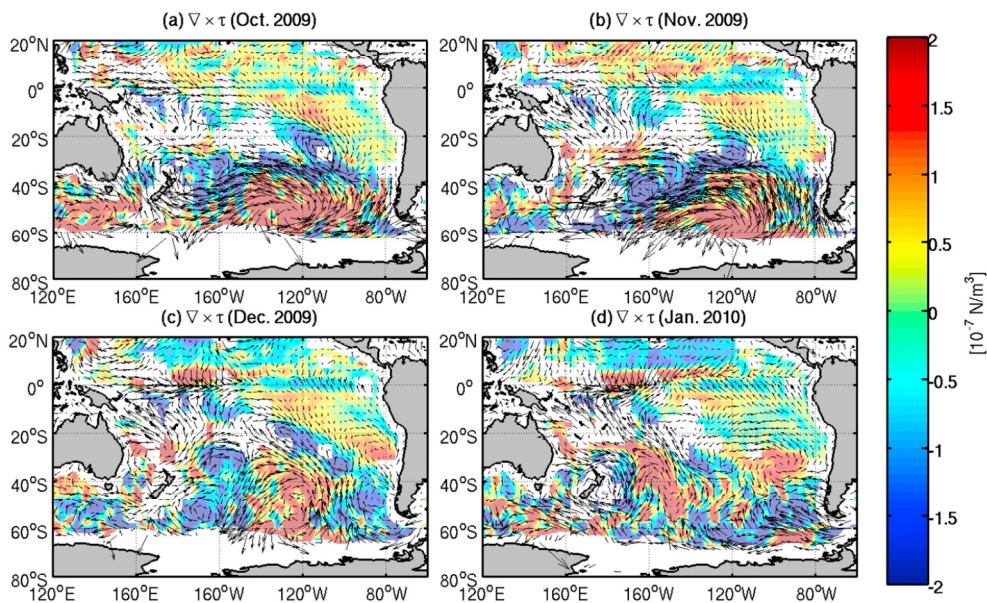


Figure 2. Monthly mean ASCAT wind stress curl anomaly (color shading) referenced to the 2007–2009 “seasonal climatology”. Overlying vectors indicate wind stress anomalies.

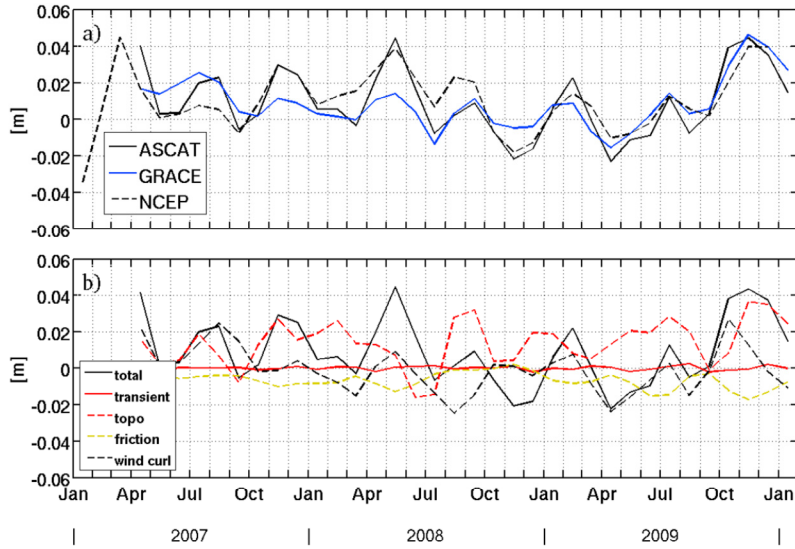


Figure 3. (a) GRACE OBP anomaly averaged over the SEP (blue). Black curves represent the estimated OBP from equation (4) using all the RHS terms. The solid and dashed black curves correspond to the use of ASCAT and NCEP for wind, respectively. (b) Contributions of relative vorticity plus vortex stretching (solid red), effects of topography (dashed red), bottom friction (yellow), as well as wind (ASCAT) and pressure forcing (dashed black) to the full reconstruction (solid black).

where η is the barotropic SSH (equivalent to OBP), $f = 2\Omega\sin(\text{latitude})$, Ω the Earth's rotation rate, $\beta = \frac{df}{dy}$, ρ the sea water density, g the local gravitational constant, r the damping or friction coefficient, τ the wind stress, P_a the sea level pressure, and H the ocean depth. The first term is the time rate of change of relative vorticity, the second is the generation of vorticity due to the stretching of the water column, the third term is the advection of the planetary vorticity gradient (beta effect), the fourth term is the advection of the vorticity induced by bottom topography (topographic effect), and the fifth term provides a damping effect. The right hand side is the forcing by wind stress curl and sea level pressure. Analysis of the relative contributions of various terms provides information about the vorticity balance that results in the observed changes in SSH and OBP.

[16] We re-arrange equation (2) into the following:

$$\frac{\partial\eta}{\partial x} = \frac{1}{\beta} \left[\frac{f}{\rho g} \nabla \times \frac{\tau}{H} - \frac{f^2}{g^2 H \rho} \frac{\partial P_a}{\partial t} - \frac{\partial}{\partial t} \nabla^2 \eta + \frac{f^2}{gH} \frac{\partial \eta}{\partial t} + \frac{f}{H} \left(\frac{\partial \eta}{\partial x} \frac{\partial H}{\partial y} - \frac{\partial \eta}{\partial y} \frac{\partial H}{\partial x} \right) - \nabla \cdot \left(\frac{r}{H} \nabla \eta \right) \right] \quad (3)$$

Integration of equation (3) along latitudinal bands in the South Pacific box westward from the eastern boundary to longitude x gives approximate values for η :

$$\eta^x = \int_{x^e}^x \frac{1}{\beta} \left[\frac{f}{\rho g} \nabla \times \frac{\tau}{H} - \frac{f^2}{g^2 H \rho} \frac{\partial P_a}{\partial t} - \frac{\partial}{\partial t} \nabla^2 \eta + \frac{f^2}{gH} \frac{\partial \eta}{\partial t} + \frac{f}{H} \left(\frac{\partial \eta}{\partial x} \frac{\partial H}{\partial y} - \frac{\partial \eta}{\partial y} \frac{\partial H}{\partial x} \right) - \nabla \cdot \left(\frac{r}{H} \nabla \eta \right) \right] dx + \eta^{xe} \quad (4)$$

where η^{xe} is the condition near the eastern boundary, chosen to be 80°W to avoid using the GRACE data that are too close to land. This “eastern-boundary” condition is east of the large OBP signal, and has little contribution to the right-

hand-side (RHS) of equation (4). Let η_*^x represent the RHS of equation (4) with all or some of the RHS terms (i.e., various approximate forms of the equation). We use the data for η , τ , P_a , and H (smoothed over $5^\circ \times 5^\circ$ to suppress small-scale contributions) to obtain η_*^x for each longitude and latitude within the SEP box. For simplicity, we refer to η_*^x as the “reconstructed” OBP. A good agreement between η_*^x (RHS) and the observed η^x (LHS) averaged within the SEP indicates the validity of the equation. We then repeat the procedure by retaining only some of the RHS terms (e.g., wind or topography) to evaluate the various approximations of the equation. Note that the reconstructed OBP is not obtained by solving for η explicitly using the equation. Because ASCAT data are only available for the period of April 2007 to April 2010, all anomalies in equation (3) are now referenced to the monthly seasonal climatology for this period (i.e., different from the seasonal climatology used to produce Figure 1).

[17] We compare time series of observed OBP anomalies η^x averaged over the SEP box (Figure 1) to the time series of the reconstructed OBP field η_*^x utilizing equation (4) averaged over the same region (Figure 3a). Relatively good agreement is found between the observed OBP time series and that based on the reconstructed OBP using all RHS terms of equation (4). For 2009 in particular, the two match very well both in amplitude and phase. The result using ASCAT wind for τ agrees with the observed amplitude of the 2009 OBP signal well using a bottom friction coefficient of 1.0×10^{-3} m/s. Note that choosing a shorter (30 day) or longer (60 day) damping time scale reduces/increases the standard deviation of the time series by 7% and 3%, respectively. This value corresponds to a damping time scale of about 45 days for a 4000 m deep ocean, which is suitable to the observed OBP anomaly and consistent with findings of Fu [2003]. The result based on NCEP wind slightly underestimates the observed 2009 OBP signal.

[18] By comparing the observed η^x with various η_*^x derived from different terms on the RHS of equation (4) and averaged over the SEP box, we can assess the relative contribution of different processes described on the RHS of equation (4). Generally speaking, the contributions by wind stress curl and topography (black and red dashed curves in Figure 3b, respectively) are the largest. Friction (yellow dashed curve) also has a significant contribution. *Fu and Davidson* [1995] and *Vivier et al.* [2005] found that the time-dependent topographic Sverdrup balance (wind stress curl balanced by the advection of planetary vorticity and topography-induced vorticity) provided a zero-order description of intraseasonal barotropic vorticity in the region. But friction was also found to be important, especially in regions with closed f/H contours (such as part of the SEP, Figure S3) where the topographic Sverdrup relation does not hold [*Webb and de Cuevas*, 2003; *Fu*, 2003; *Vivier et al.*, 2005]. Our results are therefore consistent with these previous findings. Before late 2009, wind and topography often work against each other (Figure 3b). In November 2009, however, they play comparable roles. Figure S2 suggests that the wind stress curl is large primarily south of 45°S. North of this latitude the topographic effect becomes more important. The reinforcement of the topographic effect by the wind stress curl associated with the strong anticyclone is the main reason for the record increase of OBP in late 2009. As also indicated in Figure 3b), transient effects due to the time rate of change of relative vorticity and vorticity generation by stretching the water column only have a minor contribution. The contribution by atmospheric pressure (not shown) is negligible for the monthly time scales of our investigation, consistent with the finding of *Willebrand et al.* [1980]. This is because the OBP adjustment to atmospheric pressure on time scales of days to weeks is near isostatic.

4. Conclusions

[19] GRACE observations reveal a record increase in OBP during late 2009 to early 2010 in the South Pacific that is larger than any multi-month signal in the southern hemisphere during the entire period of the GRACE data record. The GRACE data indicates that a similar signal in altimeter-derived SSH is mostly barotropic in nature. The OBP signal is found to be associated with a strong and persistent anticyclone that is unprecedented in the past three decades (Figure S2). Dynamical analysis suggests the OBP/SSH anomalies are caused by wind stress curl associated with the anticyclone and advection of planetary and topographically induced vorticity (a time-dependent topographic Sverdrup balance), but modified by friction. The re-enforcement of wind and topographic effects in late 2009 is the main reason for the record OBP anomaly. Our study is a demonstration of GRACE's capability to study sub-basin scale oceanic features.

[20] *Lee et al.* [2010] reported a record warming in the mixed layer (upper 50 m) in the South-central Pacific in late 2009 to early 2010 in the northwestern part of the extreme anticyclone. The contribution of that shallow warming to the South East Pacific (the region with the record anomaly of OBP) is, however, small, consistent with the agreement between OBP and SSH. The OBP anomaly is centered at a different location from the surface warming because it is forced by the wind stress curl and bottom topography.

[21] *Lee et al.* [2010] only discussed the related mixed-layer warming and the thermodynamical balance. The present study extends the scope of that study by investigating the related signatures in OBP and SSH, their relation to wind stress curl and topography, and the vorticity dynamics. The large atmospheric and oceanic anomalies in late 2009 in the South Pacific were believed to be fueled by the 2009–10 El Niño [*Lee et al.*, 2010] because of the record magnitude of that El Niño in the central-equatorial Pacific [*Lee and McPhaden*, 2010]. The OBP/SSH signal reflects an anomalous anticyclonic flow that would deflect the Antarctic Circumpolar Current (and the warmer waters that it carries) towards Antarctica in the same way that an atmospheric anticyclone deflects the circumpolar westerly winds (along with the warm air that it carries) southward. The potential impacts on Antarctica warrant further investigation.

[22] **Acknowledgments.** This work was supported by the NASA Physical Oceanography, Solid Earth, MEASUREs and EOSDIS Programs and performed at the Jet Propulsion Laboratory, California Institute of Technology, under contract with NASA. We thank the German Space Operations Center (GSOC) of the German Aerospace Center (DLR) for providing continuously and nearly 100% of the raw telemetry data of the twin GRACE satellites and the processing centers at University of Texas, JPL, and Geoforschungszentrum Potsdam. We also thank the two anonymous reviewers for their thorough reviews and several important suggestions.

References

- Chambers, D. P. (2006), Evaluation of new GRACE time-variable gravity data over the ocean, *Geophys. Res. Lett.*, *33*, L17603, doi:10.1029/2006GL027296.
- Chambers, D. P., and J. K. Willis (2008), Analysis of large-scale ocean bottom pressure variability in the North Pacific, *J. Geophys. Res.*, *113*, C11003, doi:10.1029/2008JC004930.
- Chambers, D. P., J. Wahr, and R. S. Nerem (2004), Preliminary observations of global ocean mass variations with GRACE, *Geophys. Res. Lett.*, *31*, L13310, doi:10.1029/2004GL020461.
- Fu, L.-L. (2003), Wind-forced intraseasonal sea level variability of the extratropical ocean, *J. Phys. Oceanogr.*, *33*, 436–449, doi:10.1175/1520-0485(2003)033<0436:WFISLV>2.0.CO;2.
- Fu, L.-L., and R. Davidson (1995), A note on the barotropic response of sea level to time dependent wind forcing, *J. Geophys. Res.*, *100*, 24,955–24,963, doi:10.1029/95JC02259.
- Kanamitsu, M., W. Ebisuzaki, J. Woollen, S.-K. Yang, J. J. Hnilo, M. Fiorino, and G. L. Potter (2002), NCEP-DEO AMIP-II reanalysis (R-2), *Bull. Am. Meteorol. Soc.*, *83*, 1631–1643.
- Lee, T., and M. McPhaden (2010), Increasing intensity of El Niño in the central-equatorial Pacific, *Geophys. Res. Lett.*, *37*, L14603, doi:10.1029/2010GL044007.
- Lee, T., W. Hobbs, J. Willis, D. Halkides, I. Fukumori, E. Armstrong, A. Hayashi, W. T. Liu, W. Patzert, and O. Wang (2010), Record warming in the South Pacific and western Antarctica associated with the strong central-Pacific El Niño in 2009–10, *Geophys. Res. Lett.*, *37*, L19704, doi:10.1029/2010GL044865.
- Macrander, A., C. Böning, O. Boebel, and J. Schröter (2010), Validation of GRACE gravity fields by in-situ data of ocean bottom pressure, in *System Earth via Geodetic-Geophysical Space Techniques*, edited by F. Flechtner et al., pp. 169–186, Springer, Berlin, doi:10.1007/978-3-642-10228-8.
- National Oceanic and Atmospheric Administration (1988), Digital relief of the Surface of the Earth, Data Announcement 88-MGG-02, Natl. Geophys. Data Cent., Boulder, Colo.
- Ponte, R. (1999), A preliminary model study of the large-scale seasonal cycle in bottom pressure over the global ocean, *J. Geophys. Res.*, *104*, 1289–1300, doi:10.1029/1998JC900028.
- Ponte, R. M., and K. J. Quinn (2009), Bottom pressure changes around Antarctica and wind-driven meridional flows, *Geophys. Res. Lett.*, *36*, L13604, doi:10.1029/2009GL039060.
- Risien, C. M., and D. B. Chelton (2006), A satellite-derived climatology of global ocean winds, *Remote Sens. Environ.*, *105*(3), 221–236, doi:10.1016/j.rse.2006.06.017.
- Smith, S. D. (1988), Coefficients for sea surface wind stress, heat flux, and wind profiles as a function of wind speed and temperature, *J. Geophys. Res.*, *93*, 15,467–15,472, doi:10.1029/JC093iC12p15467.

- Syed, T. H., J. S. Famiglietti, M. Rodell, J. Chen, and C. R. Wilson (2008), Analysis of terrestrial water storage changes from GRACE and GLDAS, *Water Resour. Res.*, *44*, W02433, doi:10.1029/2006WR005779.
- Velicogna, I. (2009), Increasing rates of ice mass loss from the Greenland and Antarctic ice sheets revealed by GRACE, *Geophys. Res. Lett.*, *36*, L19503, doi:10.1029/2009GL040222.
- Verspeck, J., A. Stoffelen, M. Portabella, H. Bonekamp, C. Anderson, and J. Figa Saldaña (2010), Validation and calibration of ASCAT using CMOD5.n, *IEEE Trans. Geosci. Remote Sens.*, *48*, 386–395.
- Vivier, F., K. A. Kelly, and M. Harismendey (2005), Causes of large-scale sea level variations in the Southern Ocean: Analyses of sea level and a barotropic model, *J. Geophys. Res.*, *110*, C09014, doi:10.1029/2004JC002773.
- Webb, D. J., and B. A. de Cuevas (2003), The region of large sea surface height variability in the southeast Pacific Ocean, *J. Phys. Oceanogr.*, *33*, 1044–1056, doi:10.1175/1520-0485(2003)033<1044:TROLSS>2.0.CO;2.
- Willebrand, J., S. G. H. Philander, and R. C. Pacanowski (1980), The oceanic response to large-scale atmospheric disturbances, *J. Phys. Oceanogr.*, *10*, 411–429, doi:10.1175/1520-0485(1980)010<0411:TORTLS>2.0.CO;2.
- Willis, J. K., D. P. Chambers, and R. S. Nerem (2008), Assessing the globally averaged sea level budget on seasonal to interannual timescales, *J. Geophys. Res.*, *113*, C06015, doi:10.1029/2007JC004517.
- Zlotnicki, V., J. Wahr, I. Fukumori, and Y. T. Song (2007), Antarctic circumpolar current transport variability during 2003–05 from GRACE, *J. Phys. Oceanogr.*, *37*, 230–244, doi:10.1175/JPO3009.1.
-
- C. Boening, T. Lee, and V. Zlotnicki, Jet Propulsion Laboratory, California Institute of Technology, 4800 Oak Grove Dr., Pasadena, CA 91109, USA. (Carmen.Boening@jpl.nasa.gov)